Astron. Astrophys. 295, 27–42 (1995)

ASTRONOMY AND ASTROPHYSICS

A sample of small size compact steep-spectrum radio sources

I. VLBI images at 18 cm

D. Dallacasa[1,2,4], C. Fanti[2,3], R. Fanti[2,3], R.T. Schilizzi[4,5], and R.E. Spencer[6]

[1] Dipartimento di Astronomia, Via Zamboni 33, I-40216 Bologna, Italy
[2] Istituto di Radioastronomia – CNR, via Gobetti 101, I-40129 Bologna, Italy
[3] Dipartimento di Fisica, via Irnerio 46, I-40126 Bologna, Italy
[4] Joint Institute for VLBI in Europe, Postbus 2, NL-7990 AA Dwingeloo, The Netherlands
[5] Sterrenwacht Leiden, Postbus 9513, NL-2300 RA Leiden, The Netherlands
[6] NRAL–Jodrell Bank, University of Manchester, Macclesfield Cheshire, SK11 9DL, UK

Received 25 May 1994 / Accepted 26 July 1994

Abstract. Global VLBI observations at 1.66 GHz of 16 powerful radio sources from the Peacock & Wall (1981) catalogue and classified as Compact Steep-Spectrum (CSS) sources are presented. These sources have, on average, higher turnover frequencies and smaller overall sizes than the CSS's selected from the 3CR catalogue. The VLBI images show other substantial morphological differences, and the scenario previously drawn for 3CR galaxies and quasars may be no longer completely valid. For example, some of the CSS galaxies in this sample have bright jets and cores, and one of them (1829+290) has $\sim$ 90% of the total flux density at this frequency coming from two nearly symmetric jets. Their overall structures can be compared with those of the compact triple sources (Conway et al. 1992). Although the galaxies in the present sample are bigger in size and not core dominated, the central component often shows a direct connection with one of the lobes, and variability is usually not observed. Quasars in this sample show a variety of morphologies, often complex or core–jet like, with compact components dominating the radio emission at this frequency.

Key words: galaxies: active – galaxies: jets – galaxies: nuclei – galaxies: quasars: general – radio continuum: galaxies

1. Introduction

CSS's are powerful radio sources with sub-galactic apparent dimensions (conventionally smaller than 15 kpc, with H_o = 100 km s^{-1} Mpc^{-1}), and a steep spectrum ($\alpha \geq 0.5$, assuming $S \propto \nu^{-\alpha}$) in the transparent regime (e.g. van Breugel 1984; Fanti et al. 1989, 1990, 1991; see also the Proceedings of the CSS/GPS Workshop 1991, for review of the CSS properties). Statistical considerations exclude the possibility that the majority of them are large sized objects seen at small angles to the line of sight and then foreshortened by projection effects (Fanti et al. 1990). Therefore they must be intrinsically small objects embedded in the ISM of the parent galaxy. They are not rare, but rather a conspicuous fraction (20% - 30%) of the high power ($P > 10^{26.5}$ W Hz^{-1}) intermediate to high redshift ($z > 0.25$) extragalactic radio source population in low–frequency source catalogues.

It has been suggested that the CSS sources may in fact be classical double radio sources in the early stages of their evolution when their jets are ploughing through the dense ISM of the host galaxies for the first time (Phillips & Mutel 1982; Mutel & Phillips 1988). VLA, Merlin, and VLBI radio observations of CSS galaxies and quasars, mainly from the 3C catalogue, show that they seem to be the small scale analogues of the large–scale classical double radio sources, showing cores, lobes, and often jets. However, they are distinguished from their large scale brethren not only by their small size, but also by frequent asymmetries in their lobes and by a high incidence of unusually distorted morphologies. Possible evolution of CSS into FR II radio sources will be discussed in a forthcoming paper (Dallacasa et al. in preparation, hereafter referred as Paper II).

These peculiarities have led to the development of a second class of models for CSS sources which proposes that they are not necessarily young, but are physically small because they are currently confined to kpc scales by an unusually dense and clumpy narrow line region which impedes the outward progression of the radio jet. This is actually observed in some nearby radiogalaxies eg. 3C299 (Liu & Pooley 1991) and 3C305 (McCarthy et al. 1991). The optical spectra of a few CSS sources show very strong emission lines, with equivalent widths in the [O III] λ5007 considerably larger than in powerful radio galaxies and radio loud quasars; this is consistent with a scenario in which CSS sources possess a substantial quantity of ionized gas

Send offprint requests to: D. Dallacasa, Dwingeloo

Table 1. CSS sources from the Peacock and Wall catalogue. Columns 1 through 11 provide: (1) name, (2) optical identification, (3) optical magnitude [inhomogeneous bands], (4) redshift, (5) linear scale factor [H_o=100 km s^{-1} and q_o= 0.5 have been assumed. A value of z = 1 has been assumed for sources without redshift], (6) maximum angular size, (7) maximum linear size, (8) flux density at 1.67 GHz, as measured by the WSRT during the VLBI observation, (9) two–point spectral index from the Peacock and Wall catalogue, (10) spectral index in the optically thin region, resulting from our fit using all the reliable data available in literature, and (11) computed turnover frequency from the same fit. We note that high frequency variability might have affected a few sources. A proper determination of the spectral index in the optically thin region should use multifrequency measurements taken at the same epoch.

Source	Opt. Id.	m	z	scale pc/mas	θ_{max} arcsec	Lin Siz kpc	S_{18} Jy	α_{5000}^{2700}	α_{thin}	ν_m MHz
0223+341	Q?	21.3		4.26	0.55	2.34	2.64	0.53	0.38	<100
0316+161	G	22.0		4.26	0.30	1.28	6.93	0.89	1.01	800
0319+121	Q	19	2.67	3.79	0.05	0.19	1.65	0.59	0.27	<100
0404+768	G	22	0.598	3.81	0.15	0.57	4.96	0.58	0.60	350
0428+205	G	20	0.219	2.25	0.25	0.56	3.58	0.50	0.67	1150
1225+368	Q	21.7	1.974	4.11	0.06	0.25	1.96	1.17	1.23	1750
1323+321	G	19.0	0.37	3.09	0.06	0.19	4.28	0.58	0.57	500
1358+624	G	19.9	0.431	3.34	0.07	0.23	3.79	0.66	0.70	550
1413+349	EF	> 23		4.26	0.06	0.26	1.63	0.60	0.84	850
1442+101	Q	17.7	3.544	3.40	0.02	0.07	2.32	0.68	0.83	1200
1600+335	Q? or G?	> 22		4.26	0.06	0.26	3.03	0.63	0.85	2400
1819+396	G	19	0.4	3.22	0.60	1.93	2.94	0.98	1.14	<100
1829+290	G	20.2	0.842	4.16	2.50	10.40	2.61	0.80	0.79	450
2230+114	Q	17.5	1.037	4.28	2.50	10.70	6.27	0.50	0.44	550
2342+821	Q	20.5	0.735	4.04	0.18	0.73	3.21	0.92	0.87	500
0345+337	G	19	0.244	2.42	0.50	1.21	1.96	0.80	0.89	< 100

energized by the active nucleus by means of jet–cloud interaction occuring in the Narrow Line Region (Gelderman 1992). The distorted and asymmetric radio morphologies observed in CSS's are hypothesized to be the manifestations of such strong jet–gas interactions (Akujor et al. 1992).

A theoretical basis for this hypothesis can be found in the numerical simulations which have shown that gas clouds can be very effective in deflecting and/or slowing outflowing plasma (Lind 1990; Balsara & Norman 1992; De Young 1991). The model for CSS sources predicts that dense knots of emission line gas will be found adjacent to bends in the radio jet and at the position of the brightest radio features (e.g., the hotspots) both in distorted and linear sources. To support this idea, optical observations with high angular resolution (such as that of the HST) in the high excitation lines are required, coupled with high resolution mapping at radio wavelengths.

In this paper we present the results of 1.66 GHz VLBI observations of 16 CSS sources. In Paper II, results obtained from VLBI observations at 6 cm of ten of the sixteen sources will be given, together with a morphological classification of the objects and a discussion of the spectral properties of the different components of each radio source.

2. The sample

The present sample includes all except two of the CSS sources from the Peacock & Wall catalogue (1981, hereafter referred to as PW) with P > $10^{26.5}$ W Hz^{-1} which are not found in the 3CR catalogue because their spectrum turns over between 150 and 5000 MHz, and their total flux density at 178 MHz is below the limit for the 3CR catalogue (10 Jy). The sources 1153+31 and 1607+26 were not observed, since sensitive VLBI observations had already been made by other groups. The PW CSS sources together with the CSS objects from the 3CR catalogue constitute a flux density and power limited sample. Many of these objects are classified as GHz-Peaked Spectrum (GPS) radio sources, similar in they properties to CSS sources (Fanti et al. 1991). The objects we observed are listed in Table 1.

We derived an optically thin spectral index for each source from a weighted least squares fit to spectral points collected from catalogues and papers in the literature. The fit was made using a hyperbolic function of the form

$$Log(S) = a \cdot Log(\nu) + b + \sqrt{c \cdot (Log(\nu))^2 + d \cdot Log(\nu) + e}$$

in the Log(ν)–Log(S) plane, with as asymptotes the optically thin and optically thick spectral indexes (Stanghellini et al. in preparation). This method allows a good determination of the turnover frequency and the spectral index in the transparent regime (see columns 11 and 10 in Table 1). Note that this determination of α_{thin} does in some cases differ from the measured α_{5000}^{2700}, possibly due to a source variability (see discussion of the individual objects).

Table 2. Observational data. The observations were performed for a total of 96 hours from 13 to 17 June 1989, with the MK II recording system, 1.8 MHz bandwidth in left circular polarization (LCP). The diameters listed for the WSRT and the VLA (in brackets) are equivalent diameters, i.e. 3 antennas for WSRT and 27 antennas for the VLA. The sensitivities of the VLA refers to a single antenna (0.089) and to the whole array (1.7).

Antenna	Diam.(m)	T_{sys} (K)	Sens. (K/Jy)
Medicina (I)	32	80	0.12
WSRT (NL)	43	70	0.3
Jodrell Bank (UK)	76	50	0.81
Haystack (US)	37	80	0.082
Green Bank (US)	43	25	0.267
Iowa (US)	18	45	0.056
Fort Davis (US)	26	65	0.10
VLA (US)	25 (130)	35	0.089 (1.7)
Pie Town (US)	25	30	0.089
Kitt Peak (US)	25	30	0.089
Owens Valley (US)	40	50	0.223

All the PW radio sources presented here have been observed with MERLIN and the VLA at several frequencies (1.67, 5 and 15 GHz).

3. Observations and data reduction

Global VLBI observations were carried out in June 1989 using the Mark II recording system (Clark 1973) and the telescopes listed in Table 2. The data were then correlated with the JPL–Caltech VLBI Correlator at the California Institute of Technology in Pasadena. Onsala and Torun did not produce fringes to the other telescopes due to equipment failures.

Every source was observed for about 1.5–2 hours of global time plus 3–4 hours for each subnetwork (EVN and USN). For about 60% of the time the VLA (in C configuration) was used in phased–array mode, enhancing the sensitivity of the observations. Flux density measurements for all sources were obtained with the WSRT at the same time as the VLBI observations. These values were used in the mapping process to check if the whole source flux density had been accounted for on VLBI scales.

The correlated data were fringe fitted in AIPS, and the flux density scale was calibrated following Cohen et al. (1975), using 0235+164 and 1404+286 (OQ208) as calibration sources, with adopted flux densities of 0.97 and 1.03 Jy. In the determination of the "$b-$factors" only baselines shorter than 20 Mλ were used since only on these baselines could both sources be assumed to be unresolved. This resulted in a separate calibration of the EVN and USN stations.

As the observations were spread over 6 days, possible variations in the gain might have affected the data, but no major effect was found, and the scatter in the $b-$factors derived from individual scans on calibrators was small ($\lesssim$ 5%), except for Haystack, for which the derived values for the $b-$factor varied, randomly with time, from twice to seven times the theoretical value for different scans on the calibrator. The system temperature (T_{sys}) measured at that station showed large variations on scales of few tens of minutes or even shorter, probably due to interference. As it was very difficult to properly track its response, we decided to discard the Haystack antenna from the data, although this increased the gap between "continental" and "transatlantic" baselines from $\sim$5 to $\sim$10 Mλ.

After the application of the $a-priori$ amplitude calibration, the data were model fitted, self–calibrated, and passed through a small number of iterations of hybrid mapping using the CORTEL algorithm (Cornwell & Wilkinson 1981). After that, they were loaded into AIPS, where the standard techniques of mapping and phase self–calibration were applied. Amplitude self–calibration was applied only once at the end of the process, using particular care; the solution interval was chosen to be longer than the scan length (30 min) in order to remove residual systematic errors and fine tune the flux density scale, but not to force the individual datapoints to follow the model. The gain corrections obtained from self–calibration were in general smaller than 2%. The rms noise level (σ) on the images, measured far from the source, is in the range 0.2 – 0.9 mJy/beam, often not far from the thermal noise ($\sim$0.17 mJy/beam for a typical observation). The dynamic range defined as peak–brightness/1σ varies from $\sim$200 to $\sim$5000.

Since all sources had MERLIN observations at this frequency (data taken in 1982, results and images published by Spencer et al. 1989), we also produced images combining these old observations with the new VLBI data, in order to have good sensitivity to relatively extended components. Great care was taken in combining the datasets in order to have the data on a common flux density scale. The integrated flux densities derived from the MERLIN images were forced to be the same as measured at Westerbork during the VLBI observations (given in Table 1). Most sources (14 out of 16) had a nearly identical conversion factor (0.94$\pm$0.02) from the MERLIN to the VLBI flux density scale. This was not true for two of them (0223+341 and 1600+335), with derived values exceeding 1. We interpret this as due to variability, with an increase of their total flux density of $\sim$ 8–10% over $\approx$7 years (1982.82 to 1989.45). However we cannot exclude that variability is present for other sources, as we are considering only two flux density measurements taken with a large time lag. Flux density variability is expected to occur only in the core of the radio source, modifying the brightness distribution between the two epochs. If variation has taken place, the combined igame may show off source noise peaks caused by the sidelobes with different intensity in the two datasets.

Images were produced with different resolving powers in order to enhance either low surface brightness components or high brightness compact features. They are shown in Figs. 1 through 22 in the form of contour plots; grey scale levels are superimposed in two cases when the contours alone are not sufficient in describing the source morphology. Image resolution, contour levels and noise are given in the captions.

4. Results and comments on individual sources

We measured flux densities and dimensions of components on the most suitable of the different resolution images, and in some case the image used for this purpose does not correspond to that shown here, which was chosen to highlight some details of the morphology.

We made the simplest interpretation of the source structure, using a "low resolution" approach. We refer to paper II for a more careful discussion of details, where we will use the full resolution of the data, and will also consider global VLBI images at 6 cm (available for 10 out of 16 sources) in order to derive spectral information for the radio components.

The numbers we derived are collected in Table 3. The labels used to identify the components are self–explanatory, based on their relative position. A comment is added into the source description if the identification of the component could be ambiguous. The criterion we adopted was to separate the components where we found angular separations larger than the beam size. Then we determined the component diameter (full width) from the images, using the lowest reliable contour (5 times the noise in the image). Exceptions were made in two cases (1413+349 and 1600+335) where bright and very compact emission is surrounded by low surface brightness emission. In Table 3 we list also extended components not detected in our VLBI images but seen on either MERLIN or VLA images, or both. Comments on individual sources give details. MERLIN flux densities were scaled by a factor of 0.94 as discussed in Sect. 3. When the difference between the sum of the flux densities of the individual components and the value measured with the WSRT is $\gtrsim 5\%$, i.e. the assumed accuracy of our amplitude calibration, this is noted in the source description.

In the following, we give a description of the morphology of each source. In these comments a reference to MERLIN and VLA images is from the results of Spencer et al. (1989).

0223+341 [Q?, m_v=21.3, z=...]

It is reported as a probable quasar by Peacock & Wall (1981), but the optical identification is still uncertain. A paper by Dunlop & Peacock (1990) describes the source as a probable galaxy, though there is no proof for this assertion.

The MERLIN image shows a triple asymmetric source of about one arcsecond in size. An EVN image at 18 cm published by Kulkarni & Romney (1991), shows a bright unresolved component and a second much fainter one, about half an arcsecond away in p.a. $\sim -120°$, corresponding to the second component seen in the MERLIN image. In our full–resolution VLBI image the SW lobe is almost completely resolved out, though there is still residual flux density of about $\sim$ 60 mJy with a peak of 4.4 mJy/beam, in the region of the second component seen by Kulkarni & Romney (1991). The bright compact emission (Fig. 1) is clearly resolved E–W and probably N–S too, though the beam is elongated in that direction and does not allow a proper separation of the different components. There are also small and faint knots in direction of the SW lobe.

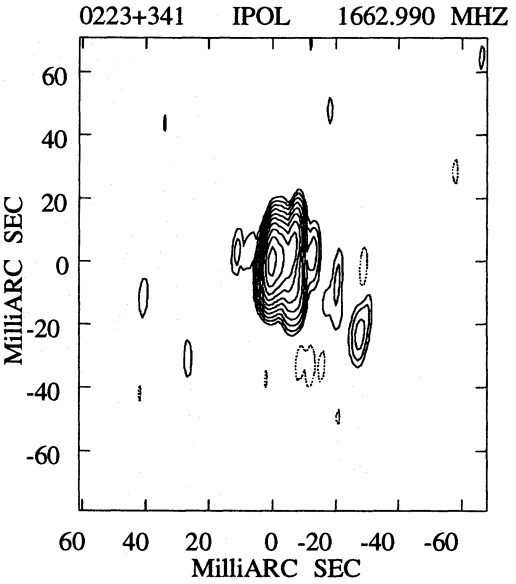

Fig. 1. HPBW = 12.8 × 2.4 mas in p.a. −4°. Contour levels are –5, 5, 10, 20, 40, 80, 150, 300, 600, 1250, 2500 times the noise of 0.28 mJy/beam. The peak flux density is 1029 mJy/beam

In a tapered image (restored with a circular beam of 30 mas) obtained using a combination of MERLIN and VLBI data (Fig. 2), the SW–lobe and a hot spot show up very clearly; the counter–lobe seen in the MERLIN image by Spencer et al. (1989), is not detected and is probably completely resolved out. The MERLIN counterlobe might be an artefact since it is not detected in our unpublished VLA A–array data at 6 cm. The overall structure is reminiscent of that seen in other CSS radio sources such as 3C286, but it looks like a small scale version of 3C273 as well.

The optically thin spectral index derived considering all the data available in the literature is α_{thin} = 0.38. However the source has been found to be variable at 18 cm (the total flux density increased by $\sim$ 8% between the MERLIN and VLBI observations), and some evidence for variability has been found at higher frequencies in the literature. Therefore we will still consider this source as being CSS until a simultaneous multi-frequency spectrum is available.

The total flux density accounted for by the two components listed in Table 3 is 2.51 Jy, i.e. 95% of value measured with the WSRT. The discrepancy could be due to the MERLIN counterlobe or be a calibration error.

0316+161 (CTA21) [G, m=22 , z=...]

This is a well known radio source, with a long history of observations over a wide range of wavelengths, from radio through X-rays, but its nature is still controversial. In particular its proposed optical identification has changed more than once; finally it has been determined to be a galaxy (Fugmann et al. 1988; Stanghellini et al. 1993). It is a non–variable radio source (Altschuler & Wardle 1976, 1977; Aller et al. 1985; Padrielli et al. 1986), with a rather flat or inverted spectrum at low frequen-

Table 3. Size and flux density of the components in the VLBI images. The columns give: (1) source name, (2) component identification, (3) and (4) major and minor axes (full width), (5) and (6) linear size corresponding to columns 3 and 4, (7) total flux density of the component.
[a] When the redshift is not available we have assumed a value of 1 in the determination of the linear size. The scale factor for each source is that given in column 5, Table 1.
[b] Component visible in the MERLIN image but fully resolved out by the VLBI baselines. The sizes are from Spencer et al. (1989), but the flux densities have been scaled as described in the text.
[c] The flux density and size of this component has been derived from Browne & Perley (1986) and Murphy (1988). See text for details.
[d] The size of the component has been derived from a fit to the image. The values reported are FWHM of the fitted Gaussian component.

Source	Comp.	θ_1 *mas*	θ_2 *mas*	Lsiz1 pc	Lsiz2 pc	S_{18} mJy	Source	Comp.	θ_1 *mas*	θ_2 *mas*	Lsiz1 pc	Lsiz2 pc	S_{18} mJy
0223+341[a]	East	15	10	60	40	2196	1413+349[a]	East	40	12	170	50	572
	West	200	100	850	425	312		Compact[d]	3	2	25	9	865
	LobeE[b]	300	200	1275	850	113		West	20	15	85	65	92
0316+161[a]	North	40	20	170	85	6456	1442+101		20	8	70	25	2264
	South	200	150	850	640	451	1600+335[a]	East	25	15	110	65	175
0319+121	VLBI	60	5	225	20	1634		Compact[d]	3	1	13	4	2233
	VLA[c]	930	640	3525	2425	30		West	30	20	130	85	453
0345+337	North	200	100	485	240	189	1819+396	North	100	50	320	160	398
	South	350	250	845	605	1577		Centre	10	4	30	12	123
0404+768	East	25	25	95	95	429		South	120	15	385	50	2159
	West	60	15	230	60	4181	1829+290	East	60	10	250	40	1221
0428+205	North	150	100	340	225	468		West	60	10	250	40	1149
	Centre	12	3	25	7	120		LobeE[b]	900	400	3750	1660	122
	South	40	20	90	45	2869		LobeW[b]	1200	900	5000	3750	150
1225+368	East	35	10	145	40	1781	2230+114	VLBI	20	10	85	40	5721
	West	10	10	40	40	139		LobeN[b]	500	300	2140	1280	75
1323+321	North	35	30	110	90	2507		LobeS[b]	300	200	1280	860	169
	South	30	25	90	75	1766	2342+821	East	30	20	120	80	80
1358+624	North	15	15	50	50	1152		Centre	30	20	120	80	174
	South	50	10	165	35	2601		West	50	40	200	160	2892

cies and a steep spectrum at frequencies higher than 1 GHz. Its radio polarization is less than 0.5 % at frequencies lower than 5GHz, increasing to a few percent at 15 GHz (Aller et al. 1985).

This object does not have a published VLBI image at 18 cm, and there are only two other VLBI images in the literature. Wilkinson et al. (1979) mapped the source at 50 cm with a resolution of 5 mas and the structure they proposed consists of a 4.6 Jy compact component < 12 mas in size, embedded in a 2.2 Jy halo (30 × 15 mas in p.a. 160°) and a 1.9 Jy fully resolved component (> 30 mas). Another model which fits the data has the same 4.6 Jy compact component plus a 4.1 Jy more extended component whose angular size in not stated in the paper. At 6cm, Jones (1984) published a hybrid map with a resolution of 5×2 mas in which the source appears as an asymmetric compact double with a separation of 12 mas, in p.a. $-10°$. Jones reports that both components are slightly resolved perpendicularly to the separation axis.

Our images at 18 cm (Figs. 3 and 4) show a peculiar morphology, which cannot be interpreted in an obvious way. The lower resolution image of Fig. 3, obtained using MERLIN and VLBI data and restored with a circular beam of 40 mas, shows a compact component corresponding to the double structure seen by Jones and displays an additional low surface–brightness, diffuse emission (roughly 200 × 100 mas in size, at a distance of $\sim$ 250 mas from the brighter component) which is detected by the shortest VLBI spacings as well as by MERLIN. It might be interpreted as the fully resolved component proposed by Wilkinson et al. (1979). It has also been detected by Spencer et al. (1989) in their 2 cm VLA image, though at this frequency it is very faint, owing to its steep spectral index. An additional compact and weak component has been found between these two at about 130 mas in p.a. $\sim 165°$ with respect to the brighter one. Its presence is confirmed by a global VLBI observation at 6 cm (see Paper II).

The dominant component mapped with maximum resolution is displayed in Fig. 4, and has its major axis in p.a. $\sim -15°$ but in addition it shows extended emission in the perpendicular direction. It could be therefore classified as a lobe.

The two components listed in Table 3 account for the total flux density.

0319+121 [Q, m=19, z=2.67]

The optically thin spectral index of this source is much flatter ($\alpha_{thin} = 0.27$) than originally found in PW, making its clas-

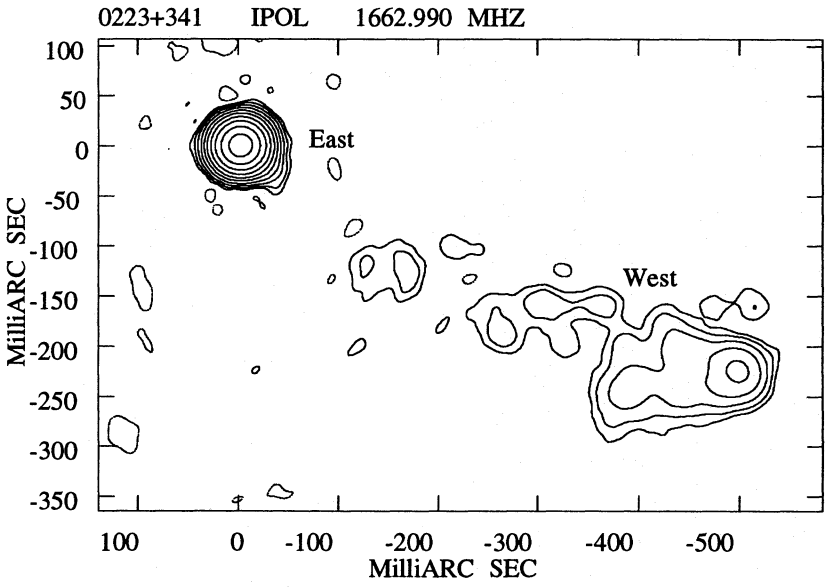

Fig. 2. Tapered MERLIN + VLBI image restored with a 30 mas circular beam. Contour levels are –5, 5, 10, 20, 40, 80, 150, 300, 600, 1250, 2500 times the noise of 0.57 mJy/beam. The peak flux density is 2090 mJy/beam

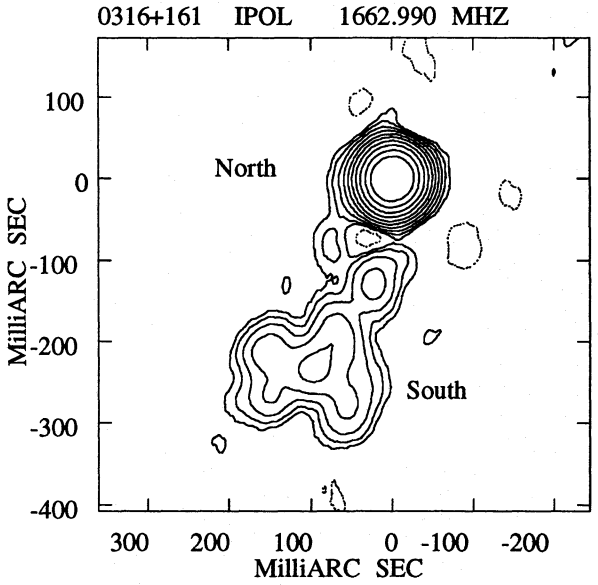

Fig. 3. Tapered MERLIN + VLBI image restored with a 40 mas circular beam. Contour levels are –5, 5, 10, 20, 40, 80, 150, 300, 600, 1250, 2500 times the noise of 0.75 mJy/beam. The peak flux density is 5908 mJy/beam

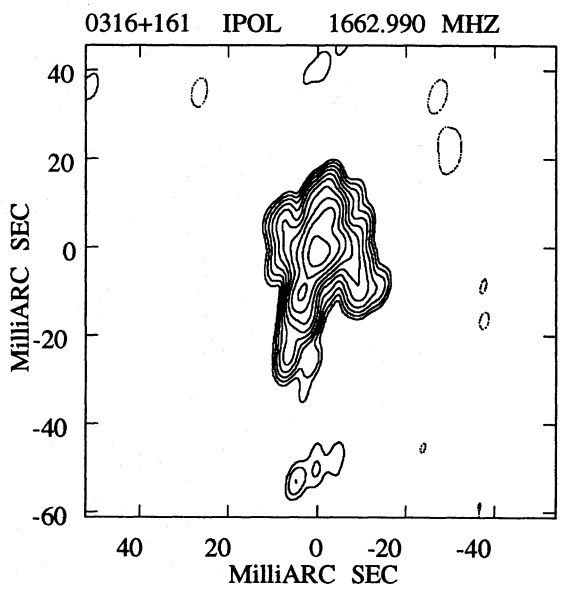

Fig. 4. VLBI–only image; the restorig beam is 6 × 3 mas in p.a. −16°. Contour levels are –5, 5, 10, 20, 40, 80, 150, 300, 600, 1250, 2500 times the noise of 0.38 mJy/beam. The peak flux density is 1464 mJy/beam

sification as a CSS questionable. This could be partly due to some intrinsic variability as seen at frequencies higher than 4.8 GHz in the flux density measurements available in the literature. However simultaneous multifrequency VLA data (Stanghellini private communication) confirm the flatness of the spectrum. No previous VLBI image is available for this object. Owing to its relatively low declination, the resolution of our data in N–S direction is rather poor. Unfortunately the source structure (see Fig. 5) is elongated in the same position angle as the beam and therefore its morphology cannot be fully interpreted using this image alone.

Super-resolving the image in the N–S direction indicates that the overall structure might be considered as an asymmetric double, although fits with two Gaussian components were not satisfactory, leaving high residuals. An image at higher frequency is needed to give a proper classification of the source, and a preliminary image obtained with global VLBI data at 6 cm shows indeed a *core* − *jet* type structure (Paper II). On larger scales, there is a faint steep–spectrum emission region about 13 arcseconds northwest of the VLBI component detected with the VLA at 21 cm by Browne & Perley (1986) and Murphy (1988), by Murhpy & Browne (1993) at 18 cm and by us at 6 cm (Paper II). It is located along the axis defined by the VLBI structure, but

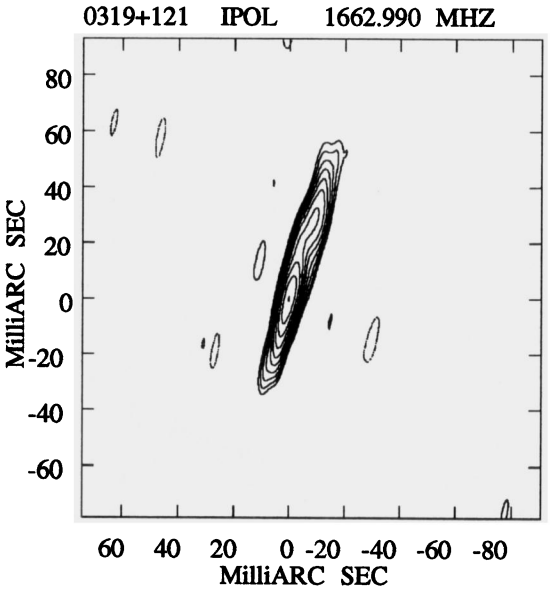

Fig. 5. VLBI image with restoring beam of 15 × 3 mas, in p.a. −12°. Contour levels are –5, 5, 10, 20, 40, 80, 150, 300, 600, 1250, 2500 times the noise of 0.36 mJy/beam. The peak flux density is 916 mJy/beam

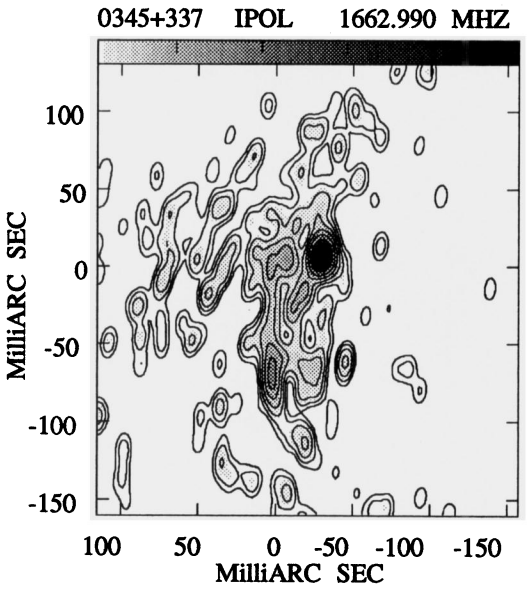

Fig. 6. VLBI–only image. The restoring beam is 14.2 × 7.1 mas in p.a. −7°. Contour levels are –5, 5, 10, 20, 40, 80, 150, 300, 600 times the noise of 0.20 mJy/beam. The peak flux density is 200 mJy/beam. The grey scale flux density range is from 2 to 100 mJy/beam

the direct relationship between the two radio emitting regions needs to be proven. Using the ratio between the flux density of the two components reported by Browne & Perley (1986) at 1.4 GHz and our measurement at 5.0 GHz, we obtain a spectral index of $\sim$ 1.6 between 21 and 6 cm. This indicates that the flux density of the lobe candidate is $\approx$30 mJy at 18 cm. The component is labelled "VLA" in Table 3, while "VLBI" refers to the structure seen in Fig. 5.

0345+337 (3C93.1) [G, m=19, z=0.244]

This source does not belong to the PW sample but it was observed because it is included in the combined sample (Fanti et al. 1990) and no VLBI image was available. Its structure was barely resolved at 18 cm in the MERLIN image. Its optical identification is with a 19^m galaxy. There is an interesting MERLIN image at 6 cm presented by Akujor et al. (1991), which shows an amorphous emission with a head-tail like shape. Pearson et al. (1985) claim the presence of a halo or a faint and relatively extended component around this object from the analysis of their VLA A-Array data at 6 cm; this component could also be responsible for the interplanetary scattering (IPS) results reported by Readhead & Hewish (1974).

In our VLBI data, the source is fully resolved on spacings longer than 20 $M\lambda$ at 18 cm. Therefore to produce the image in Fig. 6 we used only the "continental" data, obtaining a resolution roughly a factor of 3 worse than for all the other sources. The source structure is unusual, and is dominated by a relatively bright but resolved component (FWHM $\sim$ 7 mas) from which departs a bifurcated curved feature which finally points to a somewhat diffuse tail. In this image there is no evidence for a core component.

The image in Fig. 6 accounts for only about 60 % of the total flux density measured with the WSRT. This is in fact the maximum flux density detected in the shortest VLBI baseline (VLA–Pie Town). The MERLIN data were thus very important in recovering the missing flux density and in producing an image with enough sensitivity to detect the diffuse, low surface-brightness emission, as displayed in Fig. 7, and completely resolved out by the VLBI spacings. This image has been produced using the AIPS task SDCLN which is more accurate in reproducing extended emission. We also tried produce an image using the Maximum Entropy Method by means of the AIPS task VTESS, but the final image was contaminated by ripples.

The overall structure is rather complex and asymmetric, reminiscent of 3C343 and 3C287 (Nan Rendong et al. 1988). It looks rather like a lobe containing a compact hot–spot, although we need to study its spectral index to confirm this interpretation and rule out the possibility that it is the source core.

The total flux density accounted for by these two regions is $\sim$ 90% of the value measured with the WSRT. This missing flux density is due to larger scale emission detected by MERLIN, but which is not properly restored in our images.

0404+768 [G, m=22, z=0.598]

An EVN image at 18 cm presented by Kulkarni & Romney (1991) shows an asymmetric double structure. The main component is elongated in the same position angle as the major axis of the radio source, that is $\sim$ 45°.

This object is very interesting when studied at higher resolution (Fig. 8: the image is rotated CCW by 45°). It shows a more complex structure than found by Kulkarni and Romney,

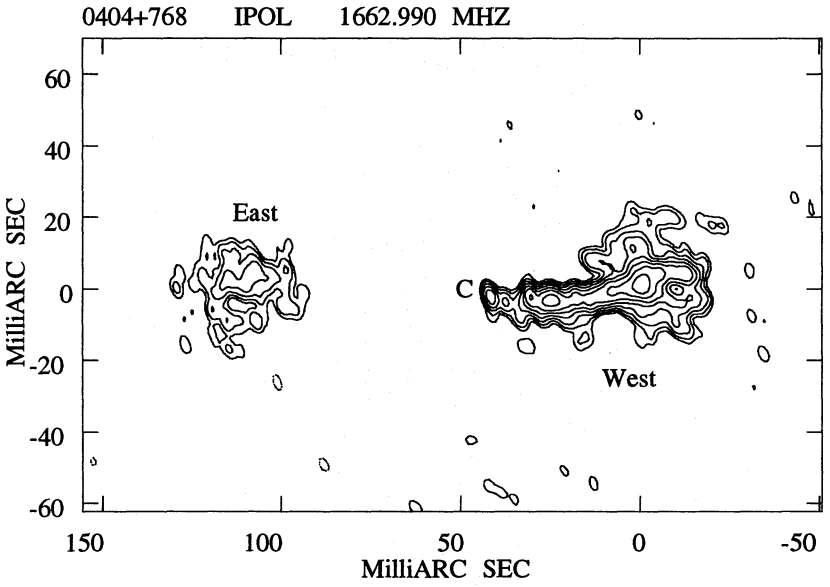

Fig. 8. The restoring beam is 4.32 × 2.29 mas in p.a. −25°. The image is rotated CCW by 45°. Contour levels are –5, 5, 10, 20, 40, 80, 150, 300, 600 times the noise of 0.40 mJy/beam. The peak flux density is 431 mJy/beam

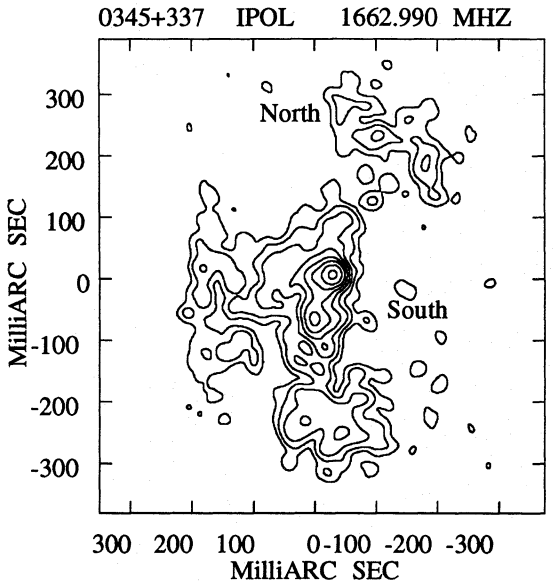

Fig. 7. MERLIN + VLBI image restored with a 25 mas circular beam. Contour levels are –5, 5, 10, 20, 40, 80, 150, 300, 600 times the noise of 0.43 mJy/beam. The peak flux density is 307 mJy/beam

dominated by a bright jet pointing to a relatively extended lobe. Such bright jets are rather unusual in the 3CR CSS radio galaxies. It has nearly constant transverse size and brightness, with little evidence of knots or gaps, though they can be partially hidden by the resolution. The jet is straight and it is not clear where it ends, because there is some "collimated emission" on the other side of the brightness peak at the centre of the brighter lobe. Tentatively we identify the core with the most compact component located at the northeastern end of the jet (indicated with a C on the image), just near the centre of the source. A similar hypothesis for 0404+768 is also advanced by Polatidis (1993).

In the image shown in Fig. 8, about 7 % of the total flux density at this frequency is missing. A tapered image, obtained including MERLIN data (not shown here), shows some diffuse structure beyond the brightest lobe although the flux density and surface brightness are quite low, and are insufficient to allow a proper evaluation of its extent.

The total flux density in the eastern lobe determined in our images is considerably lower than that determined by Kulkarni and Romney from their EVN data. Even assuming that the flux density missing from Fig. 8 is related to that component, some 250 mJy are still needed to get to their value. However image is in good agreement with that shown by Polatidis (1993) at the same frequency, although we cannot detect his additional weak diffuse emission south of the western lobe.

0428+205 [G, m=20, z=0.219]

There are two published VLBI images at 18 cm, by Phillips and Mutel (1981) and by Waak et al. (1987), but with lower resolution and sensitivity than the present data. The MERLIN image shows a barely resolved source, slightly extended in the N–S direction. The VLA image at 2 cm in Spencer et al. (1989) clearly resolves the radio emission into two separate components (see Fig. 1h in their paper). The VLBI image in Fig. 9 reproduces only the southern part of the source. Most of the flux density comes from a very complex structure, which could be interpreted as a lobe. At about 30 mas in p.a. $\sim -30°$ there is fainter elongated component of about 120 mJy, which basically confirms the second component seen also by Waak et al. (1987). Some 450 mJy are missing in the present image, though they are partially sampled in the shortest VLBI baseline.

Figure 10 shows an image obtained using both MERLIN and VLBI data, and restored with a circular beam of 10 mas. An additional diffuse component, accounting for the missing flux density, is visible. Should the core turn out to be located in the region of the 120 mJy component (termed Centre in Table 3),

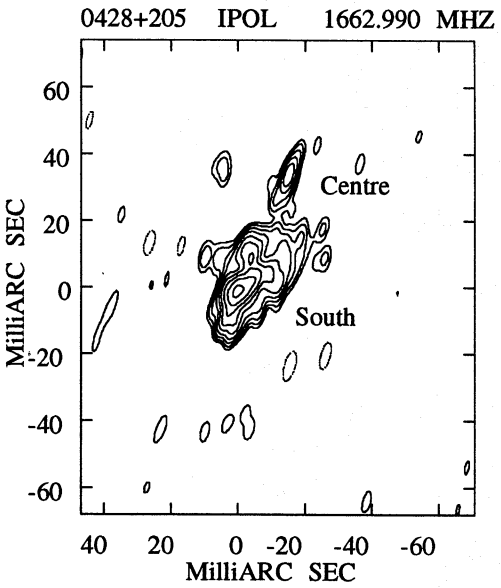

Fig. 9. VLBI–only image. The restoring beam is 6.19 × 2.43 mas in p.a. −15°. Contour levels are –5, 5, 10, 20, 40, 80, 150, 300, 600, 1250 times the noise of 0.45 mJy/beam. The peak flux density is 696 mJy/beam

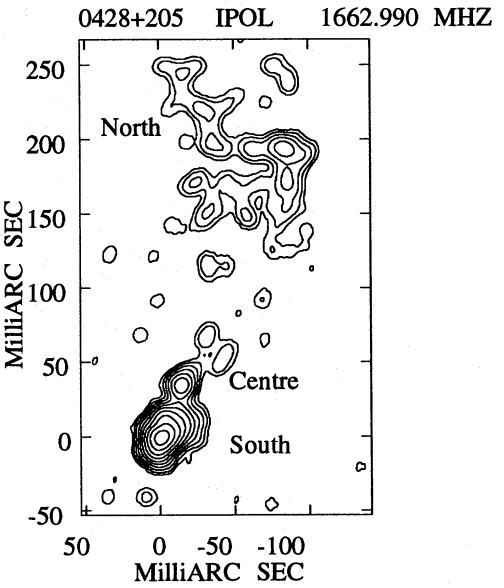

Fig. 10. MERLIN + VLBI image, restored with a circular beam of 10 mas. Contour levels are –5, 5, 10, 20, 40, 80, 150, 300, 600, 1250, 2500 times the noise of 0.39 mJy/beam. The peak flux density is 1476 mJy/beam

this source would be a very asymmetric double, similar to other more extended CSS sources (e.g. 3C49, 3C299), though this object is somewhat more compact.

1225+368 [Q, m=21.7, z=1.974]

The information in the optical band on this object is very sparse, and the redshift has been measured only recently by Xu et al. (1993). The optical identification was with a stellar object (Peacock et al. 1981), but Polatidis (1993) reports it as a quasar.

There is a VLBI image obtained from USN VLBI data at 18 cm and published by Hodges et al. (1984), showing an asymmetric double source. They report a separation of 18 mas in p.a. −80°, but that structure is only part of what is imaged with the present data (see Fig. 11). In fact the emission is dominated by a jet like structure ∼ 30 mas in size, and there is an additional component lying at about 55 mas in p.a. ∼ −90° with respect to the dominant easternmost component, chosen as reference.

It is a quite peculiar source because its structure can be easily separated into different discrete components. Gaussian fits gave very good results, and all the components align within few degrees in p.a. −87°. The image of the residuals after the Gaussian components have been removed has the same noise level as the off–source noise measured far from the radio emission. This would mean that there is no underlying continuous emission as in most jets, or at least it has an extremely low surface brightness. The image in Fig. 11 accounts for all the flux density of the source, which is the same as derived by adding the integrated flux densities of the individual Gaussian components. The radio emission might originate in a chain of well defined shocks caused by a supersonic jet.

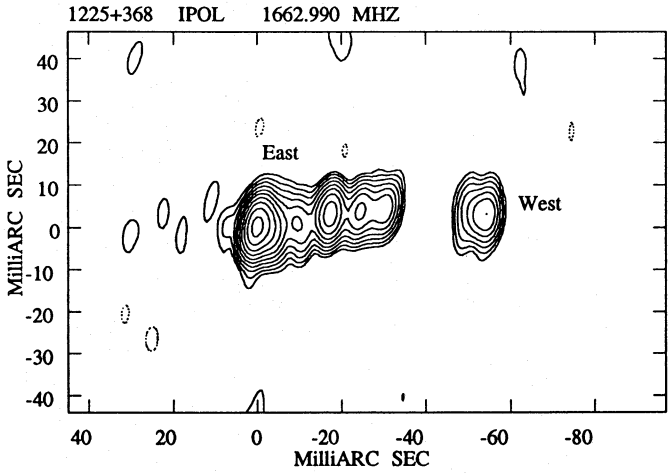

Fig. 11. The restoring beam is 7.0 × 3.0 mas in p.a. −8°. Contour levels are –5, 5, 10, 20, 40, 80, 150, 300, 600, 1250, 2500 times the noise of 0.23 mJy/beam. The peak flux density is 776 mJy/beam

It is unclear which component can be identified as the core. The sizes derived for each component are similar. This source has a very steep spectrum ($\alpha \sim 1.2$) in the optically thin region, and this may be interpreted as an indication that a flat-spectrum core is not of great significance. In Table 3 parameters are given for the two patches of emission labelled East and West in Fig. 11 only; a more detailed discussion will be given in Paper II.

1323+321 (DA344) [G, m=19, z=0.37]

An image at 18 cm obtained from USN VLBI data by Mutel & Phillips (1981), shows a nearly symmetric double, with a

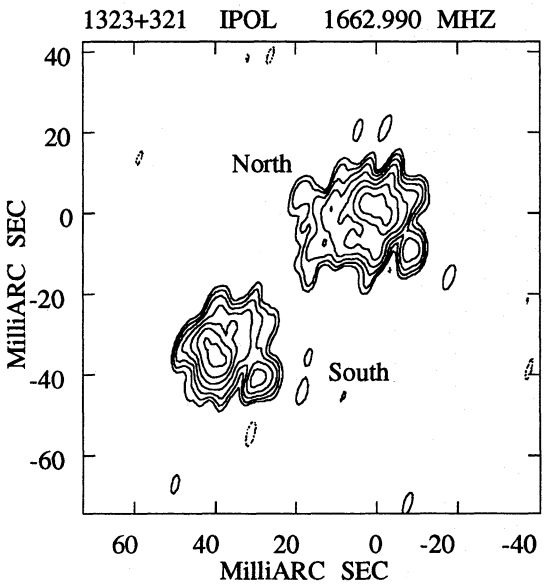

Fig. 12. The restoring beam is 5.822 × 2.23 mas in p.a. −13°. Contour levels are –5, 5, 10, 20, 40, 80, 150, 300 times the noise of 0.65 mJy/beam. The peak flux density is 316 mJy/beam

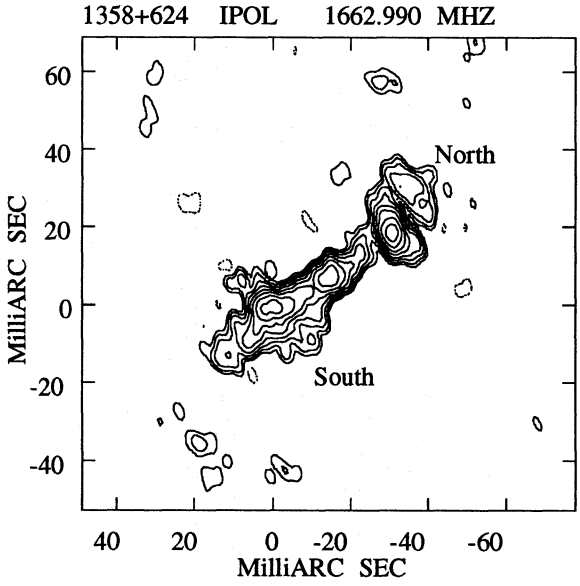

Fig. 13. VLBI image with restoring beam of 4.21 × 2.23 mas, in p.a. 20°. Contour levels are –5, 5, 10, 20, 40, 80, 150, 300, 600 times the noise of 0.37 mJy/beam. The peak flux density is 355 mJy/beam

separation of 55 mas, in p.a. ∼ 50°. Both components appear partially resolved.

The image produced with the present data (Fig. 12) shows the source morphology in more detail: the two components appear as resolved lobes with complex morphology. The uv−coverage at short spacings is rather poor, and this is particularly true around 3–4 Mλ, the region of the uv−plane sensitive to source structure scales with the size of the lobes. Therefore the quality of the image presented here is lower than for most other sources (for more exhaustive considerations about image reliability versus uv−coverage, see Fanti et al. 1985).

There is no indication of the identification of the core, not even in EVN + USN VLBI data at 6 cm (Stanghellini private communication). This source is the prototypical example of the Compact Double class of radio sources (Mutel et al. 1988).

The antisymmetric morphology is suggesting of gravitational lensing effects. A detalied study of the spectral index distribution should be carried out confirm this suggestion.

1358+624 [G, m=19.9, z=0.431]

This radio source is a known low frequency variable. A 50 cm VLBI image by Padrielli et al. (1991), shows double structure with the lobes connected by a rather faint bridge. Our image (Fig. 13) shows a similar morphology, with the bridge clearly identified as a jet; the structure accounts for all the flux density of the radio source at this frequency. Note that the components at the edges of the radio source are broadened in different directions. A fit to the northern and most compact region with a single Gaussian was not satisfactory, and revealed a well resolved component with underlying more extended emission. Preliminary results from VLBI data at 6 cm show that this region has a steep spectrum and appears extended in the same way as the present data, ruling out its identification as a core. The component labelled North in Table 3 refers to the brightest spot at the northern end of the image and also includes the diffuse emission in p.a. ∼ −20°, while South accounts for the jet–like structure.

An optical image of this source is published by Stanghellini et al. (1993) and reveals the presence of obscuring material in a direction roughly perpendicular to the VLBI axis, but on larger scale.

1413+349 [EF, m> 23, z=...]

This object has no optical identification; Stanghellini et al. (1993) set a limit of 24^m and 23^m on its optical emission in the r and i bands respectively. O'Dea et al. (1992) marginally detected it in the IR, and give a $18^m.8$ in the K band, and infer therefore that the identification is with a very red object ($r - K \gtrsim 4.2$).

The radio source has been mapped by Hodges et al. (1984) at 18 cm using USN VLBI data, and the source structure was interpreted as a core–jet. Our image (Fig. 14) shows a compact component (Centre, the core candidate) and two-sided emission with the eastern jet dominating over the western. The more diffuse western component can also be seen in the image by Hodges et al., although they did not comment on it. This extended component, in p.a. ∼ −70° with respect to the core candidate, contains 92 mJy (∼ 5%) of the total flux density of the source at this frequency. It could be a counter–jet or a lobe.

The jet to the NE is straight and well–collimated. It is unclear whether it ends in a hot-spot or it fades away in the faint knots of emission extending beyond the bright spot. The size of the East component (jet) we list in Table 3 has been taken considering the outernmost knot. In the image we can account

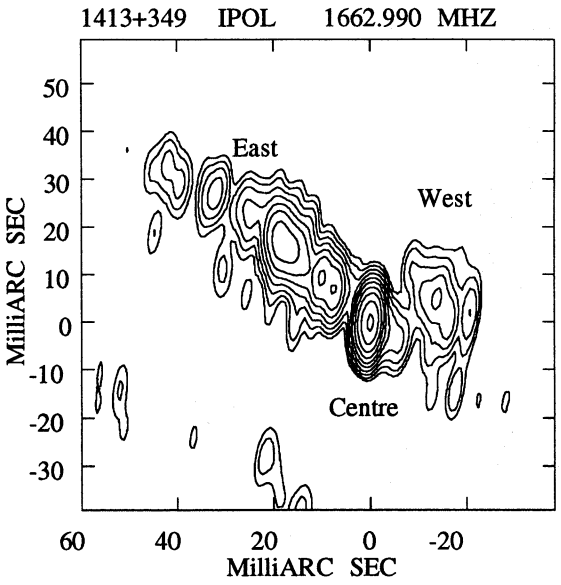

Fig. 14. VLBI image with restoring beam of 8.01 × 2.27 mas, in p.a. −9°. Contour levels are −5, 5, 10, 20, 40, 80, 150, 300, 600, 1250, 2500 times the noise of 0.20 mJy/beam. The peak flux density is 575 mJy/beam

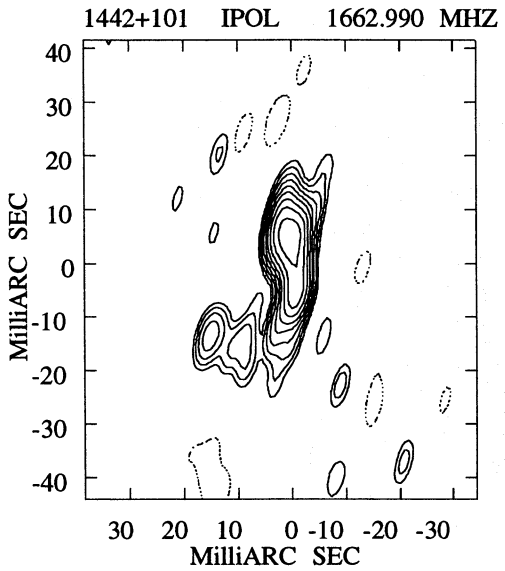

Fig. 15. VLBI image with restoring beam of 6.34 × 2.42 mas, in p.a. −15°. Contour levels are −5, 5, 10, 20, 40, 80, 150, 300, 600, 1250 times the noise of 0.34 mJy/beam. The peak flux density is 734 mJy/beam

for only 94% of the total flux density, but we could not find any additional component either in the MERLIN or a tapered combined image. In Table 3 we separate the source into three parts because the radio emission is dominated by the bright component (labelled "Compact" in Table 3) containing ∼ 53% of the total flux density, which is only marginally resolved on the longest spacings and is partially connected to the other regions in our contour image of Fig. 14.

1442+101 (OQ 172) [Q, m=17.7, z=3.544]

This object has the highest redshift in our sample. It is unresolved by MERLIN and there is no previous VLBI image, although Marcher & Shaffer (1980) provide a model to their three baseline VLBI observations at 18cm. Our image (Fig. 15) shows a very small object (∼ 70 pc, the smallest in our sample), extended roughly in the N–S direction with parameters in good agreement with those given by Marscher and Shaffer. Several fits in terms of a number of Gaussian components have been attempted, but none was satisfactory. Therefore we interpret the extended emission to the south as a continuous structure, and tentatively classify this object as a core–jet, the core being in the northern part of the radio emission. An image obtained at 6 cm using the antennas at Medicina, Noto and Onsala (Bondi et al. in preparation), shows only a compact component of ∼ 900 mJy, which could be identified with the core candidate, although we cannot say where it is located in the image in Fig. 15. Global VLBI data at 5 GHz by Gurvits et al. (in preparation) shows a bright compact component and a short and much weaker jet–like feature in p.a. ∼ 0°, suggesting that the core is located at the southern end of the source. In that case, however, the jet would have an extremely steep-spectrum.

1600+335 [Q? or G?, m> 22, z=...]

This object is classified as a radio loud quasar (Impey & Tapia 1991), although there is no reference for its optical identification available in literature. Stanghellini et al. (1993) have found the optical object to be "extended", and therefore a galaxy, but their detection was based on a convolution of their optical image, because no significant optical emission has been found at full resolution.

In the radio band it has been mapped by Kulkarni & Romney (1991). Their image obtained from EVN data at 18 cm shows a compact component with some extended emission in the EW direction. In our image (Fig. 16) the emission is dominated by an unresolved component embedded in a diffuse halo. There is also a low surface brightness emission region at about 40 mas in p.a. ∼ 90° corresponding to the eastern tail seen by Kulkarni and Romney.

The interpretation of the morphology of this source is not simple. The compact component could be considered as either the core or a bright hot–spot. There is no indication of jets on the mas scale, and the extended emission could be also considered in terms of two quite asymmetric lobes.

The source is variable; its flux density at 1.67 GHz increased by about 10 % between the MERLIN and VLBI observations. At higher frequencies even stronger variations appear to take place. In 1991 we measured the flux density at 5 GHz with the VLA as being 2.6 Jy, which is about 30 % higher than that reported in the VLA calibration manual, and about 60 % higher than the value measured by Wall & Peacock (1985) at the same frequency. This variability makes us favour the core rather than hot–spot interpretation of the compact component discussed above.

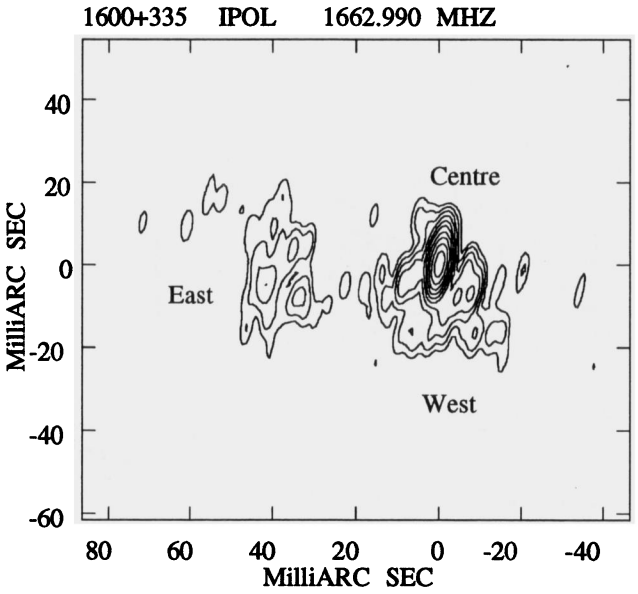

Fig. 16. VLBI image with restoring beam of 6.95 × 2.21 mas, in p.a. −11°. Contour levels are –5, 5, 10, 20, 40, 80, 150, 300, 600, 1250, 2500 times the noise of 0.41 mJy/beam. The peak flux density is 1785 mJy/beam

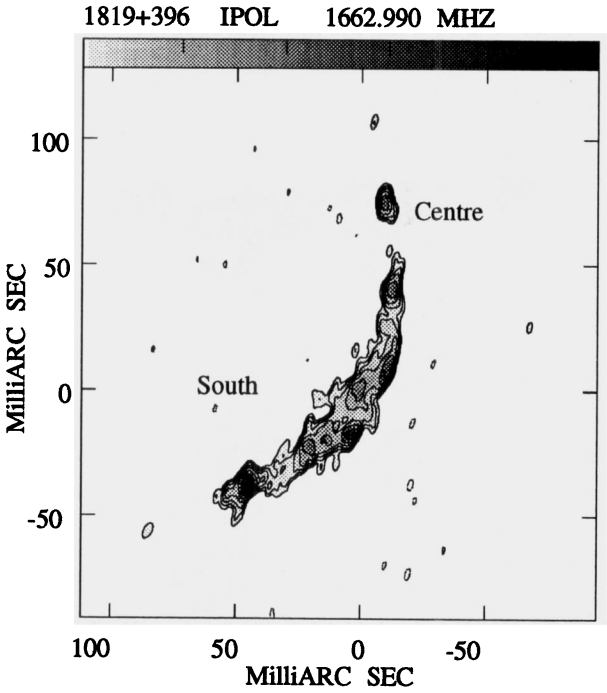

Fig. 17. VLBI image with restoring beam of 5.24 × 2.18 mas, in p.a. −14°. Contour levels are –5, 5, 10, 20, 40, 80, 150, 300 times the noise of 0.39 mJy/beam. The peak flux density is 196 mJy/beam. The grey scale flux density range is from 2 to 100 mJy/beam

In Table 3, we have considered three components for this source: that termed "Centre" has been extracted from the larger-sized West emission by means of a Gaussian fit. It accounts for ∼ 74% of the total flux density. In the image presented in Fig. 16, about ∼ 5% of the total flux density is missing. This could be due to more extended emission, probably related to one of the diffuse components, which is too small to be adequately sampled by the MERLIN, but too large for VLBI spacings we obtained.

1819+396 [G, m=19, z=0.4]

The MERLIN image at 18 cm resolves the source into two asymmetric components separated by half an arcsecond, in p.a. ∼ −27°. The image obtained by Kulkarni & Romney (1991) from EVN data at 18 cm, shows a "banana-shaped" region corresponding to the brighter component of the MERLIN image, while the second component is completely resolved out. In our image (Fig. 17) the brighter component in the MERLIN image is resolved into a curved arch, possibly a bent jet, with compact components at both extremities. It is not possible to identify which of the two is the core, though the southern one appears more compact. This source is very interesting because the jet can be studied in great detail, being resolved perpendicularly to its axis. The grey scale plot superimposed on the contours in Fig. 17 allows a better identification of the details in the jet structure. Limb brightening effects are clearly present (as in M87, Reid et al. 1989) and the surface brightness increases where the jet bends are more prominent, as seen in the jets of some extended radio sources studied with the VLA (see for example the main jet in 1919+479, Burns et al. 1986).

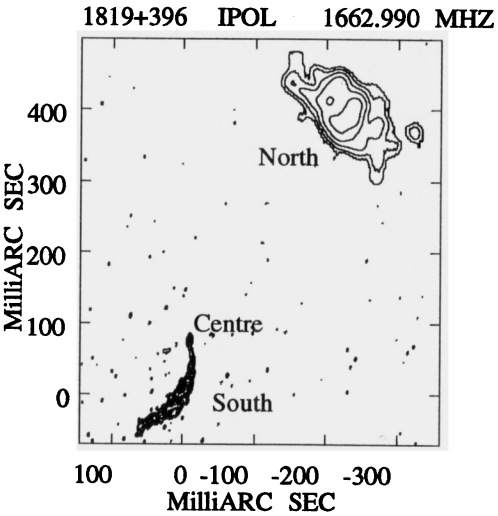

Fig. 18. VLBI + MERLIN : The southern component has been restored with a beam of 5.2 × 2.2 mas in p.a. −14°, while the northern component has been restored with a circular beam of 20 mas. Contour levels are –5, 5, 10, 20, 40, 80, 150, 300 times the noise of 0.36 mJy/beam. The peak flux density is 198 mJy/beam

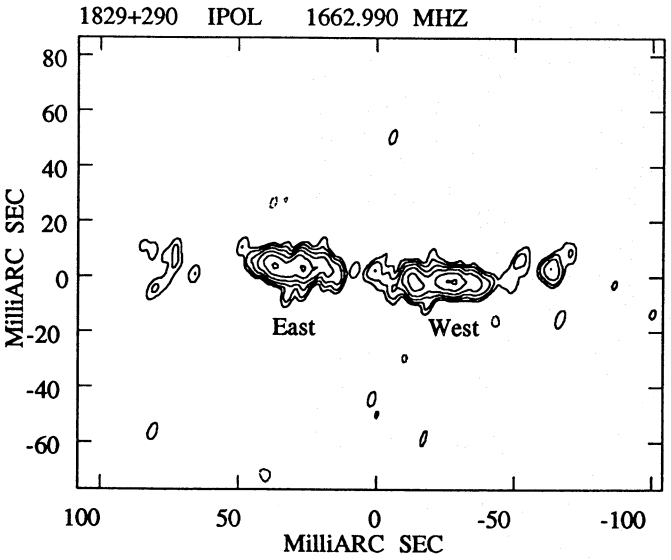

Fig. 19. VLBI image with restoring beam of 6.0 × 3.0 mas, in p.a. −17°. Contour levels are –5, 5, 10, 20, 40, 80, 150 times the noise of 0.89 mJy/beam. The peak flux density is 143 mJy/beam

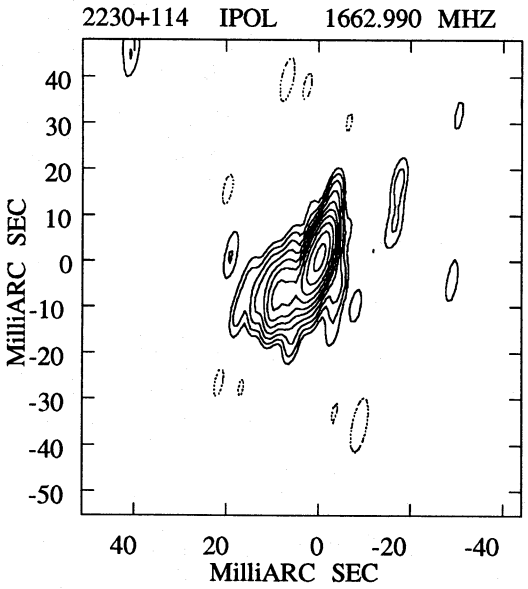

Fig. 20. VLBI image with restoring beam of 8.49 × 2.42 mas, in p.a. −11°. Contour levels are –5, 5, 10, 20, 40, 80, 150, 300, 600, 1250, 2500 times the noise of 0.91 mJy/beam. The peak flux density is 2973 mJy/beam

The northern component is nearly completely resolved out by most of the VLBI spacings, but it shows up when using combined MERLIN and VLBI data. The image obtained in this way (Fig. 18) has been cleaned and restored with two different beams. The jet has been deconvolved and restored using the maximum resolution allowed by the present data, whereas the extended lobe has been deconvolved and restored with a larger beam obtained by convolving the "original" dirty and clean beams with a circular Gaussian having HPBW = 20 mas (and applying a normalization factor). About ∼ 8% of the total flux density is not accounted for in our images. The considerations made for 1600+335 apply to this source too.

1829+290 [G, m=20.2, z=0.842]

A recent paper by Stickel & Kühr (1993), changed the original optical identification of this object to a galaxy. Previously it was believed to be a high redshift quasar as reported in Spencer et al. (1989). Dunlop & Peacock (1990) had already turned the optical identification to G?, though no proof for such change was presented. The MERLIN image at 18 cm of this object shows a compact component and two faint lobes in p.a. 53° and −115° on either sides at 1.2 and 1.4 arcsec., similar both in size and flux density and containing about 12% of the total flux density at this frequency (122 and 150 mJy, respectively). Their spectral index derived from the data published in Spencer et al. (1989) are ∼ 1.7 and ∼ 1.9.

No VLBI image is available in literature. The image presented here (Fig. 19) displays a rather symmetric source similar to the much larger FR–I radio galaxies classed as "naked jets". The radio emission is dominated by a pair of bright elongated features (jets) in p.a. ∼ 90° containing 86% of the total flux density, and therefore, within the errors, all the flux coming from the compact component seen with MERLIN. Their flux density ratio is about 1.1:1, the eastern part being more luminous. The large misalignment of these jets with respect to the outer lobes is remarkable. The source is completely resolved out by spacings longer than $20M\lambda$, and there is no clear core candidate detected in these data. We tentatively interpret the structure as a pair of symmetric jets, although there is no proof since we do not detect the radio core. The size of the jets reported in Table 3, was determined using a tapered image in which they are connected with the faint emission on either side.

If this interpretation is correct, the object is rather unusual as it is not common to find two-sided VLBI jets. Only a few other examples are known in both low luminosity radio galaxies (e.g. 3C338, Feretti et al. 1993) and high luminosity objects (3C236, Schilizzi et al. 1988; see also the new class of compact symmetric objects outlined in Wilkinson et al. 1993 and Readhead et al. 1994).

2230+114 (CTA102) [Q, m=17.5, z=1.037]

Its high–frequency spectral index turns out to be slightly below the chosen border line of 0.5 and the source is a known variable, both in structure and flux density, so perhaps this is not a typical CSS source. Many other properties (see Rantakyrö et al. 1994) make the classification difficult, as it is a powerful emitter in all bands from the radio through to the γ–rays.

The MERLIN image at 18 cm displays two asymmetric outer lobes: the brighter has ∼ 170 mJy and is at 1.6 arcsec in p.a. 143° with respect to the compact emission. The counterlobe has 75 mJy and is at 1 arcsec in p.a. −43°. The spectral indices

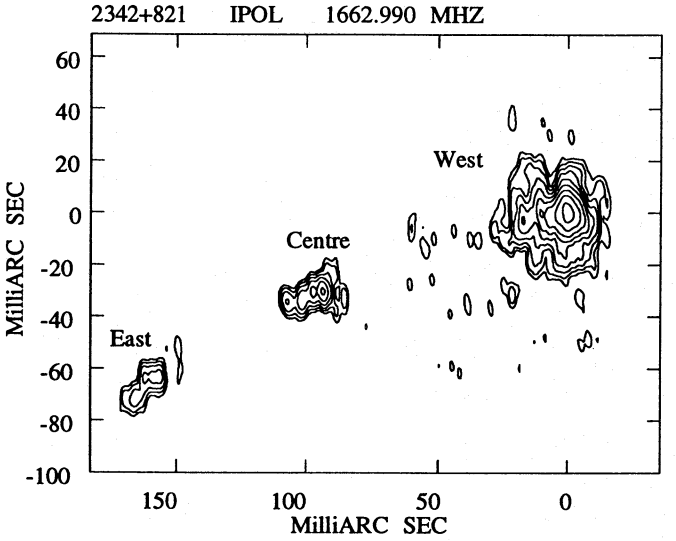

Fig. 21. VLBI image with restoring beam of 7.14 × 2.29 mas, in p.a. 6°. Contour levels are –5, 5, 10, 20, 40, 80, 150, 300, 600, 1250 times the noise of 0.25 mJy/beam. The peak flux density is 480 mJy/beam

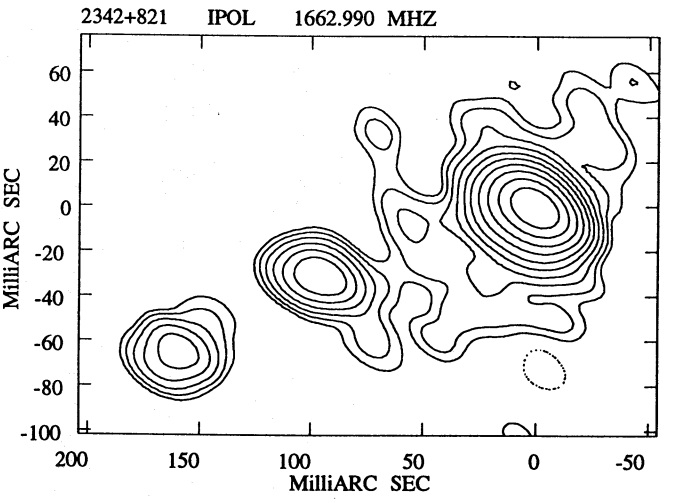

Fig. 22. VLBI + MERLIN image with restoring beam of 21.7 × 11.9 mas, in p.a. 54°. Contour levels are –5, 5, 10, 20, 40, 80, 150, 300, 600, 1250, 2500 times the noise of 0.37 mJy/beam. The peak flux density is 1773 mJy/beam

between 18 and 6 cm are ~ 0.7 and ~ 0.3 respectively (Spencer et al. 1989).

The main lobe has also been mapped with the VLA by Rusk (1988) and has an elongated shape in the direction of the source axis, suggesting that it has an arcsecond–scale jet. Several authors have published VLBI images at different frequencies and resolutions, and it is claimed to be a superluminal source (e.g. Bååth 1987). At 6 cm, VLBI observations by Wehrle & Cohen (1989) resolve the compact component in the MERLIN image into three main components and a diffuse curved tail which points toward the east implying a considerable misalignment with respect to the arcsecond–scale structure.

Our image (Fig. 20) is very similar to that found by Bååth at 932 MHz. A two Gaussian component fit gave a separation of 12.6 mas, but the residual image is more consistent with a compact component plus continuous structure, like the jet found at 6 cm by Wehrle & Cohen (1989), rather than with the two separate knots model as proposed by Bååth. However the resolution of our data is insufficient to allow a proper comparison with the Wehrle and Cohen data.

Taking into account the two components detected by the MERLIN and the VLBI structure of Fig. 20, about 5% of the total flux density is still missing, due either to additional structure not adequately sampled by our data or to the accuracy of the amplitude scale.

2342+821 [Q, m=20.5, z=0.735]

No previous VLBI image is available, and the MERLIN data show only a point–like component.

Our image (Fig. 21) obtained using VLBI data only, displays a well aligned triple object whose emission is dominated by a large component representing ~ 90% of the total flux density. This is most likely a lobe, accompanied by two other spots of emission nearly aligned in p.a. ~ +130° at a distance of ~ 100 and ~ 160 mas from the dominant lobe. Their interpretation is not obvious: each of them could either contain the source core or be knots in a jet. Figure 22 displays the image obtained adding the MERLIN data and restored with a larger beam. The dominant component shows a tail in the direction of the two other components, confirming the lobe interpretation. Assuming that the central component is the core, the source becomes a very asymmetric triple, but this interpretation needs to be confirmed by spectral information. A similar conclusion is reported by Polatidis (1993), who shows an image very similar to ours.

5. Discussion

In the following, we briefly discuss the conclusions which can be drawn from the VLBI images presented here. The 16 sources studied here show a great variety of morphology, and some of them could be compared with extended radio sources seen on larger scales with the VLA. The emission of some objects is dominated by a very bright lobe (e.g. 2342+821) or a prominent jet (1819+396), while in a few cases, the core candidate represents the dominant component (1600+335).

The jets are generally rather bright, and their occurrence and relevance in galaxies is more frequent than in 3CR CSS galaxies. Some of the jets are at least partially resolved perpendicularly to their major axis, and therefore they can be studied in the same way as the kpc-scale jets imaged with the VLA or the WSRT. A more complete analysis of this aspect will be given in a forthcoming paper (Paper II).

In contrast to the 3CR sample of CSS sources, the PW CSS galaxies have a higher incidence of core candidates (e.g. 0404+768 and 0428+205). The radio galaxies from the 3CR are dominated by the lobe emission and with core flux density much

less than 1% of the total at high frequencies (van Breugel et al. 1984, 1992; Sanghera 1993).

5.1. *Evidence of interaction with the ambient medium ?*

The images of many of these objects show distorted or complex morphologies (0223+341, 0316+161, 0428+205, 1600+335, 1819+396, 2230+114), which can be interpreted as being due to interaction between the radio emitting plasma and the ambient medium. Additional evidence for interaction comes from the high excitation observed in the optical spectra of a sample of 15 (3CR) CSS sources (Gelderman 1992). The high [O III] luminosities and broad profiles show the presence of a substantial amount of ionized gas possibly energized by the radio jets originating in the nuclei. Such jets can accelerate the clouds in the Narrow Line Region to the velocities needed by the broad line profiles observed, significantly broader than those observed in other AGN types (Gelderman 1992).

5.2. *Sizes*

PW CSS's are smaller on average than 3CR CSS's, as expected for sources with synchrotron self–absorption occurring at higher frequency. If we consider a simple model in which the radio source expands and increases the size of its emitting components progressively with time, younger objects with smaller total linear size can be expected to have components which are more compact and therefore have higher turnover frequency. None of the sources listed here has known extended emission on a few arcsecond scales, namely on linear sizes greater than the diameter of a typical galaxy, except, perhaps 0319+121. Another source in our sample, 1323+321, is claimed to have an extended halo (Rusk 1988), a few arcseconds in size, but our VLBI image accounts for all the flux density at this frequency, so we can set an upper limit to the flux density of this component at 1.67 GHz of 5%, corresponding to the assumed error in our flux density scale. Therefore the dominant radio emission for the CSS sources presented here comes from sub–kpc regions and presumably from the same volume as the NLR of the parent object.

5.3. *Confinement*

At present we do not have any direct measurements or estimates of the physical conditions of the ambient gas in the objects studied here. As stated above, the VLBI emitting regions are generally within $\approx$ 1 kpc of the nucleus of the parent object, and therefore we can assume that the physical conditions of the ambient medium are the same as in the NLR. Assuming the typical values for temperature and density as inferred from optical observations of standard (nearby) AGNs, namely $T = 10^4$ K and $n = 10^{4\pm1}\mathrm{cm}^{-3}$ (from Netzer 1991), for the NLR clouds, and $T = 10^7$ K and $n = 1$ cm^{-3} (Canizares et al. 1987) for the intercloud medium, we can derive a value of $10^{-8} - 10^{-9}$ dyne/cm^{-2} for the static pressure of the ambient medium of the radio emitting plasma. Such values are not sufficient to confine the radio emitting components, which have minimum internal pressures 4 or 5 orders of magnitudes higher, as calculated from parameters in Table 3 (see also Paper II), and assuming equipartition (Pacholczyk 1970). Therefore, if the sources are confined by means of the static pressure of the ambient gas, we have to assume that either the physical conditions in the nuclear regions of the CSS are more extreme than in typical AGNs (higher particle density and/or higher temperature). In this case we should expect X-ray emission at higher levels than usually observed. This hypothesis is consistent with the "frustrated" or "smothered" radio source model (Baum et al. 1990; Schilizzi 1991; Stanghellini et al. 1993) in which the CSS and GPS radio sources are confined on sub-kpc scales by an intrinsically very dense medium, or by infalling matter as a consequence of a merger or of a close encounter with a companion. Alternatively it is possible that the radio sources are expanding and that the ram pressure can balance the internal pressure. This may not be required for the cores or core candidates but it has to be effective for the lobes and jets, and requires expansion velocities of 100 km s^{-1} or more. In this case the radio source can expand as the components find themselves in lower density regions with a corresponding decrease in radio luminosity.

Further evidence for the importance of the insterstellar medium comes from the radio polarization measurements. Polarization of the CSS-GPS sources is generally very low ($\lesssim$ 0.5%) at 5 GHz (Stanghellini et al.; Lüdke et al. in preparation). Results in this field are rather sparse, but for some objects there are indications that the fractional polarization increases at high frequency (see the case of CTA21 which becomes significantly polarized at 15 GHz). This may be due to beam depolarization effects, because at least for the sources of the present sample their structures were not resolved with the VLA. But in any case, the ionization produced by the supposed strong jet–medium interaction would provide free electrons which in turn would produce Faraday rotation and depolarization, and these processes are less effective at high frequencies.

6. Summary

VLBI images with linear resolutions ranging from $\sim$5 to $\sim$ 10 pc have been presented for 16 sources belonging to a high frequency sample of Compact Steep-Spectrum radio sources. Their morphologies differ from those seen for the sources selected from the low frequency 3CR catalogue. In particular, objects identified with galaxies in this sample are characterized by a high fraction of the total flux density coming from jets and core candidates, in strong contrast to 3CR CSS galaxies.

The optical counterparts of these objects are fainter than the 3CR sources, and some of them present evidence for obscuring matter (Stanghellini et al. 1993). This probably implies a higher density and temperature in the nuclear regions which in turn can explain the smaller sizes as the ambient medium more efficiently impedes the expansion of the radio emitting plasma.

There is certainly good evidence for strong interaction between the radio components and the NLR medium.

Acknowledgements. We thank the European VLBI Network and the United States VLBI Network for carrying out the observations. We are particularly grateful to the Caltech Block-2 Correlator personnel for carefully correlating this large experiment. The WSRT is operated by the Netherlands Foundation for Research in Astronomy with the financial support of the Netherlands Organization for Scientific Research (NWO). The National Radio Astronomy Observatory is operated by Associated Universities, Inc., under contract with the National Science Foundation. This research has made use of the NASA/IPAC Extragalactic Database (NED), which is operated by the Jet Propulsion Laboratory, California Institute of Technology, under contract with the National Aeronautics and Space Administration. We thank Dr. M. Stickel and Dr. H. Kühr for providing a manuscript prior to publication. DD acknowledges the Commission of the European Union for the award of a Fellowship.

References

Akujor, C.E., Spencer, R.E., Zhang, F.J. et al., 1991, MNRAS, 250, 215.
Aller, H.D., Aller, M.F., Latimer G.E. et al., 1985, ApJS, 59, 513.
Altschuler, D.R., Wardle, J.F.C., 1976, MemRAS, 82, 1.
Altschuler, D.R., Wardle, J.F.C., 1977, MNRAS, 179, 153.
Bååth, L.B., 1987. In: Zenzus, J.A., Pearson, T.J. (eds.) Superluminal Radio Sources. Cambridge Univ. Press, Cambridge, p.206.
Balsara, D.S., Norman, M.L., 1992, ApJ, 393, 631.
Baum, S.A., O'Dea, C.P., Murphy, D.W. et al., 1990, A&A, 232, 19.
van Breugel, W.J.M., Miley, G.K., Heckman, T.M., 1984, AJ, 89, 5.
van Breugel, W.J.M., 1984. In: Fanti, R., Kellermann, K.I., Setti, G. (eds.) Proc. IAU Symp. 110, VLBI and Compact Radio Sources. Reidel, Dordrecht, p. 59.
van Breugel, W.J.M., Fanti, C., Fanti, R. et al., 1992, A&A, 256, 56.
Burns, J.O., O'Dea, C.P., Gregory, S.A. et al., 1986, ApJ, 307, 73.
Canizares, C.R., Fabbiano, G., Trinchieri, G., 1987, ApJ, 312, 503.
Clark, B.G., 1973, Proc. IEEE, 61, 1242.
Cohen, M.H., Moffet, A.T., Romney, J.D. et al., 1975, ApJ, 201, 249.
Conway, J.E., Pearson, T.J., Readhead, A.C.S. et al., 1992, ApJ, 396, 62.
Cornwell, T.J., Wilkinson, P.N., 1981, MNRAS, 196, 1067.
De Young, D.S., 1991, ApJ, 371, 69.
Dunlop, J.S., Peacock, J.A., 1990, MNRAS, 247, 19.
Fanti, C., Fanti, R., Parma, P. et al., 1985, A&A, 143, 292.
Fanti, C., Fanti, R., Parma, P. et al., 1989, A&A, 217, 44.
Fanti, R., Fanti, C., Schilizzi, R.T. et al., 1990, A&A, 231, 333.
Fanti, C., Fanti, R., O'Dea, C.P., Schilizzi, R.T. (eds.) 1991, Compact Steep–Spectrum & GHz–Peaked Spectrum Radio Sources. Bologna: Istituto di Radioastronomia–CNR.
Feretti, L., Comoretto, G., Giovannini, G. et al., 1993, ApJ, 408, 446.
Fugmann, W., Meisenheimer, K., Röser, H.J., 1988, A&AS, 75, 173.
Gelderman, R., 1992. Jet–Gas Interactions in Compact Steep–Spectrum Radio Sources. In: Burgarella, D., Livio, M., O'Dea, C.P. (eds.) Poster Papers from the Space Telescope Science Institute Symposium *Astrophysical Jets.* STI preprint, Baltimore, p. 16
Hodges, M.W., Mutel, R.L., Phillips, R.B., AJ, 89, 1327.
Impey, C.D., Tapia, S., 1990, ApJ, 354, 124.
Jones, D.L., 1984, ApJ, 276, L5.
Kulkarni, V.K., Romney, J.D., 1991. VLBI Observations of CSS Selected at 2700 MHz. In: Fanti, C., Fanti, R., O'Dea, C.P., Schilizzi, R.T. (eds.) Compact Steep–Spectrum & GHz–Peaked Spectrum Radio Sources. Bologna: Istituto di Radioastronomia–CNR, p.85.
Lind, K.R., 1990. In Zenzus, J.A., Pearson, T.J. (eds.) Parsec-scale Radio Jets. Cambridge Univ. Press, Cambridge, p. 274.
Marscher, A.P., Shaffer, D.B., 1980, AJ, 85, 668.
McCarthy, P.J., van Breugel, W.J.M, Kapahi, V. K., 1991, ApJ, 371, 478.
Murphy, D.W., 1988, Ph.D. Thesis, Univ. of Manchester.
Murphy, D.W., Browne, I.W.A., 1993, MNRAS, 264, 298.
Mutel, R.L., Phillips, R.B., Skuppin, R., 1981, AJ, 86, 1600.
Mutel, R.L., Phillips, R.B., 1988. In: Reid, M.J., Moran, J.M. (eds.) Proc. IAU Symp. 129, The impact of VLBI on Astrophysics and Geophysics, Kluwer Academic Publishers, Dordrecht, p. 73.
Netzer, N., 1991. AGN Emission Lines. In: Courvoisier J.J.L., Major, M. (eds.) Saas-Fee Advanced Course 20, Active Galactic Nuclei. Springer, Berlin, 57.
O'Dea, C.P., Davies, J.K, Stanghellini, C. et al., 1992. In Holt, S.S., Neff, S.G., Urry, C.M. (eds.) AIP Conf. Proc., No. 254, Testing the AGN Paradigm, American Institute of Physics, New York, p. 435.
Pacholczyk, A.G., 1970, Radio Astrophysics, Freeman and Co., San Francisco.
Padrielli, L., Aller, M.F., Aller, H.D. et al., 1986, A&AS, 67, 63.
Padrielli, L., Eastman, W., Gregorini, L. et al., 1991, A&A, 249, 351.
Peacock, J.A., Wall, J.V., 1981, MNRAS, 194, 331.
Peacock, J.A., Perryman, M.A.C., Longair, M.S. et al., 1981, MNRAS, 194, 601.
Pearson, T.J., Perley, R.A., Readhead, A.C.S., 1985, AJ, 90, 738.
Phillips, R.B., Mutel, R.L., 1981, ApJ, 244, 19.
Phillips, R.B., Mutel, R.L., 1982, A&A, 106, 21.
Polatidis, A.G., 1993, PhD Thesis, Univ. of Manchester.
Rantakyïo, F.T., Bååth, L.B., Dallacasa, D. et al., 1994, A&A, submitted.
Readhead, A.C.S., Hewish, A., 1974, MemRAS, 78, 1.
Readhead, A.C.S., Xu, W., Pearson, T.J. et al., 1994. In Zensus, J.A., Kellerman, K.I. (eds.) Compact Extragalactic Radio Sources. Green Bank, National Radio Astronomy Observatory, p. 17.
Reid, M.J., Biretta, J.A., Junor, W. et al., 1989, ApJ, 336, 112.
Rusk, R.E., 1988, PhD Thesis, Univ. of Toronto.
Sanghera, H.S., 1993, PhD Thesis, Univ. of Manchester.
Schilizzi, R.T., 1990. Introduction to the Workshop. In: Fanti, C., Fanti, R., O'Dea, C.P., Schilizzi, R.T. (eds.) Compact Steep–Spectrum & GHz–Peaked Spectrum Radio Sources. Bologna: Istituto di Radioastronomia–CNR, p.1.
Schilizzi, R.T., Skillman E.D., Miley, G.K. et al., 1988. In: Reid, M.J., Moran, J.M. (eds.) Proc. IAU Symp. 129, The impact of VLBI on Astrophysics and Geophysics, Kluwer Academic Publishers, Dordrecht, p. 127.
Spencer, R.E., McDowell, J.C., Charlesworth, M. et al., 1989, MNRAS, 240, 657.
Stanghellini, C., O'Dea, C.P., Baum, S.A. et al., 1993, ApJS, 88, 1.
Stickel, M., Kühr, H., 1993, A&AS, 101, 521.
Xu, W., Lawrence, C.R., Readhead, A.C.S. et al., 1994, AJ, 108, 395.
Waak, J.A., Spencer, J.H., Simon, R.S. et al., 1987. In: Reid, M.J., Moran, J.M. (eds.) Proc. IAU Symp. 129, The impact of VLBI on Astrophysics and Geophysics, Kluwer Academic Publishers, Dordrecht, p. 141.
Wall, J.V., Peacock, J.A., 1985, MNRAS, 216, 173.
Wehrle, A.E., Cohen, M.H., 1989, ApJ, 346, L69.
Wilkinson, P.N., Readhead, A.C.S., Anderson, B. et al., 1979, ApJ, 232, 365.
Wilkinson, P.N., Polatidis, A.G., Readhead, A.C.S. et al., 1993. In Davis, R.J., Booth, R.S. (eds.), Subarcsecond Radio Astronomy, Cambridge Univ. Press, p. 213.